J. Fluid Mech. (1996), vol. 328, pp. 297–311

Layer formation in monodispersive suspensions and colloids

By A. E. HOSOI[1] AND TODD F. DUPONT[2]

[1]The James Franck Institute and Department of Physics, The University of Chicago, 5640 S. Ellis Ave., Chicago, IL 60637, USA

[2]The Department of Computer Science, The University of Chicago, 1100 E. 58th St., Chicago, IL 60637, USA

(Received 15 February 1996 and in revised form 20 July 1996)

We present theoretical results on spontaneous stratification of sedimenting suspensions and colloids caused by a lateral temperature gradient. Fluid motion is treated in the Stokes approximation, and motion of suspended particles is described by Burgers equation with convection. The internal structure and interaction of shocks at convection roll boundaries is studied numerically using a reduced one-dimensional model based on a Galerkin approach. Qualitative comparison is made to experimental data.

1. Introduction

For over a century, it has been observed that an initially uniform suspension will develop multiple layers of varying concentrations (Brewer 1884; Mendenhall & Mason 1923; Mason & Mendenhall 1923). This phenomenon is of potential interest for industrial applications and possibly geological processes as well (Siano 1979). Stratification is observed even in monodispersive (all particles the same size) suspensions and in colloids with specially coated particles which exclude all but hydrodynamical interparticle interactions (Siano 1979). The crucial factor is the presence of a lateral temperature gradient.

In this paper we describe these layered structures in a monodispersive system. We find that each 'shock' is the line separating two adjacent convection rolls; this is a detailed description of the scenario suggested in Mendenhall & Mason (1923) and Mason & Mendenhall (1923). Multiple rolls and strata in a monodispersive system can be induced by special initial conditions with stretched gradients of particle concentration. We begin by analysing thermal convection in the presence of a lateral temperature gradient. Then this problem is combined with sedimentation of a monodispersive system described by Burgers equation (Barker & Grimson 1987; Saarloos & Huse 1990; Esipov 1995; Whitham 1974). To study the interaction of shocks, the resulting system is reduced to one spatial dimension using a Galerkin approximation which also sheds some light on the internal structure of the layer. These reduced equations are then solved numerically with a finite difference scheme. We briefly mention some convergence studies, and finally, the results are compared with experimental data.

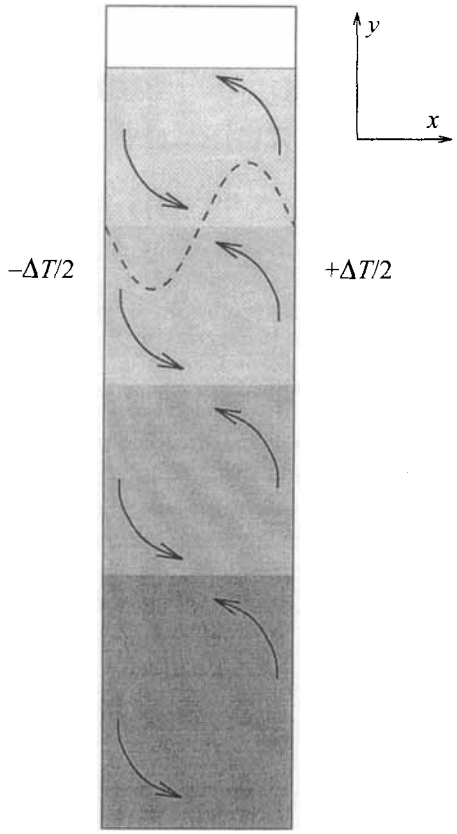

FIGURE 1. A schematic diagram of the system. Light areas represent high concentrations of particles and dark areas show low concentrations. The arrows indicate convection rolls. The dashed line represents the velocity test function used in the Galerkin approximation (see §4).

2. Brief description of the phenomenon

When an initially homogeneous colloidal suspension is left to settle, multiple layers with different concentrations are observed. This phenomenon has been documented in a wide range of materials and in both sedimenting and creaming particles (Brewer 1884; Siano 1979; Mueth *et al.* 1996). More recently, it has been shown (Mueth *et al.* 1996) that there is a convection cell in each layer apparently driven by a small horizontal temperature gradient $\approx 0.01°C$ (see figure 1). This suggests that the interaction between convection and sedimentation is essential in forming and stabilizing the layers. Experiments in Siano (1979) were performed on monodispersive colloids, while Mueth *et al.* (1996) refers to polydispersive mixtures. To simplify matters we will discuss solely the creaming case, but the sedimentation case is analogous.

The typical experimental scales include (Mueth *et al.* 1996) test tubes ≈ 25 cm high and $1 - 2$ cm in diameter. The beads that form the system have a radius of about 10^{-4} cm. The solution generally starts out with a uniform concentration (Siano 1979; Mueth *et al.* 1996), and a small volume fraction of beads, $\approx 10^{-4}$, or with a uniform concentration gradient (Siano 1979); multiple layers take days or weeks to develop. Care must be taken that the temperature gradient across the tube does not get too large since even radiated body heat is enough to destroy the layers.

3. Formulation of the model

Let us consider thermal convection of a fluid between two parallel vertical plates (two-dimensional geometry) separated by a distance $2d$ and maintained at temperatures $T_0 \pm \Delta T/2$. In such a geometry, fluid cannot be in equilibrium; any temperature difference across the 'tube' will drive a convection roll. The relevant temperature gradients and convection speed, u, are assumed small, in the sense that the inequalities $Re \ll 1$, $RePr \ll 1$ are satisfied. Here the Reynolds and Prandtl numbers are given by $Re = ud/\nu$ and $Pr = \nu/\chi$, with ν and χ being viscosity and thermal diffusivity of the fluid, respectively. We assume that thermal transport is essentially independent of convection, and the lateral temperature profile is linear, given by $T(x, y) = T_0 + \Delta T x/2d$, where $x \in [-d, d]$ is the horizontal coordinate and y is the vertical one.

To study thermally induced motion we treat fluid with particles as an effective medium. This description is justified at scales of order d provided that the convection velocity, $\boldsymbol{u}$, greatly exceeds the velocity of creaming, $\boldsymbol{v}_0$ (see below). Inside the strata where $\boldsymbol{u}$ is much greater than $\boldsymbol{v}_0$ this description is valid. We are dealing with small Reynolds numbers and time scales greatly exceeding settling times of viscous flows, which allows us to use Stokes approximation (Landau & Lifshitz 1987). Then the equations of motion for an incompressible fluid in the presence of gravity $\boldsymbol{g}$, become

$$\nabla p = \rho(\nu \Delta \boldsymbol{u} + \boldsymbol{g}), \tag{3.1}$$

$$\nabla \cdot \boldsymbol{u} = 0. \tag{3.2}$$

We neglect the viscosity dependence on particle volume fraction, c, and temperature. However, in the forcing term we need to retain the c and T dependence. To leading order we get

$$\frac{\nabla p}{\rho} = \nu \Delta \boldsymbol{u} + \frac{\Delta \rho}{\rho} c \boldsymbol{g} - \frac{x}{2d} \beta \Delta T \boldsymbol{g}. \tag{3.3}$$

Here $\Delta\rho$ is the density difference between particles and the surrounding fluid, ρ is the density of fluid (with or without particles to this order), β is the coefficient of thermal expansion. To arrive at (3.3) one assumes that the fluid velocity field adjusts instantaneously to the slowly changing c-field. The velocity field $\boldsymbol{u}$ vanishes at the boundaries.

In the absence of particles, $c = 0$, (3.3) is linear and the solution reflects only thermal convection

$$v = -\frac{g\beta\Delta T}{12\nu d}\left(x^3 - xd^2\right), \qquad u = 0, \tag{3.4}$$

where $\boldsymbol{u} = (u, v)$. This solution is valid far from the bottom and top of the sedimenting system and describes up and down motion in a single convection roll. A single roll becomes unstable to multiple rolls when convective heat transfer is no longer negligible with respect to heat conduction. This happens at $GrPr \approx 1$ where the Grashof number, Gr, is defined as $Gr \equiv \beta \Delta T g d^3/\nu^2$. Here $Gr \approx 10$. Under the experimental conditions of interest the formation of multiple rolls requires the presence of particles.

We now consider the motion of particles. It is sufficient for our purposes to use the Burgers equation description (Burgers 1974; Barker & Grimson 1987; Saarloos & Huse 1990; Esipov 1995) with advection. We assume that the drift of particles is due to fluid convection and buoyancy hindered by particle interaction. The latter is described in the dilute limit by Batchelor's formula (Batchelor 1972). The mass conservation equation reads

$$c_t + \boldsymbol{u} \cdot \nabla c + \boldsymbol{v}_0 \cdot \nabla(1 - kc)c = D \Delta c, \tag{3.5}$$

here $\boldsymbol{v}_0 = 2a^2\Delta\rho\boldsymbol{g}/9\rho_0\nu$ is the velocity of an isolated particle of radius a when buoyancy is balanced by Stokes drag, k is a constant, D is the particle diffusivity. For colloids, $D = k_B T/6\pi\rho_0\nu a$ is the Brownian diffusivity; for suspensions, D corresponds to the empirical description of hydrodynamical diffusivity (Nicolai *et al.* 1995; Esipov 1995). The dependence of diffusivity on c is neglected. For colloids in which thermal motion keeps the local distribution of particles random, Batchelor's work (Batchelor 1972) shows that k is approximately 6.55. For suspensions k is 10–20% smaller. Regularizing forces such as surface charge may also lead to different values of k. The numerical results presented here were run with k between 2 and 7.

When particles are present uniformly and *do not move* with respect to the surrounding fluid (in the limit $v_0, D \to 0$) the same convection roll is established. Interesting behaviour begins when the initial concentration field is not uniform. When a temperature gradient is added there are two factors that contribute to the lateral density profile of the fluid: temperature and particle concentration. Levels of equal density begin to flatten out and multiple convection rolls may form. Experimentally, the interface between layers is observed to be tilted. We can account for this by balancing hydrostatic pressure with the forcing due to temperature. Within the layers, the temperature forcing term is primarily balanced by viscous shear. However, near each shock, the velocity runs parallel to the interface so the two important effects are temperature and hydrostatic pressure, $p = \Delta\rho g d \tan\phi$, where $\Delta\rho$ is the density difference between two adjacent layers and ϕ is the tilt angle. Equating these two terms (pressure and forcing due to ΔT) in (3.3), using d as a characteristic length scale, and assuming $\phi \ll 1$, we can estimate a relationship for ΔT and ϕ:

$$\Delta T \sim \frac{2\Delta\rho\phi}{\beta\rho}. \tag{3.6}$$

This also gives us an upper bound for ΔT. If ϕ gets too large, $\phi \sim O(1)$, the layer will be destroyed. Thus $\Delta T_{\max} \sim 2\Delta\rho/\beta\rho$.

As suggested by Mendenhall & Mason (1923) 'both a temperature and a density gradient are necessary to produce stratification'. We can estimate the initial size of the convection rolls by balancing these two effects. We start with an initial positive concentration gradient in the y-direction; then there is a density difference in the y-direction due to concentration and in the x-direction due to temperature. The lateral density difference will immediately force a convection roll which will shift the concentration of particles. The fluid reaches a steady state when lateral concentration density differences exactly cancel temperature density differences. This is easily achieved away from the boundaries since low concentrations (more-dense fluid) are being pulled up on the warm side and pushed down on the cool side (see figure 2). However, near the top and bottom of the domain particles are being moved across the tube; this motion cannot create a sufficient lateral concentration gradient to compensate for the temperature difference. Thus we can estimate the size of the initial roll by matching density differences:

$$\Delta\rho^x = \beta\Delta T\rho \approx \Delta\rho^y = \Delta\rho\, c_y|_{init}\, \Delta y. \tag{3.7}$$

Here $\Delta\rho$ is the density difference between particles and fluid, and the subscript denotes a derivative. The approximate size of the initial convection roll, H_{roll}, is given by

$$H_{roll} \sim \frac{\Delta y}{2} = \frac{\beta\Delta T\rho}{2\Delta\rho}\left(c_y|_{init}\right)^{-1}. \tag{3.8}$$

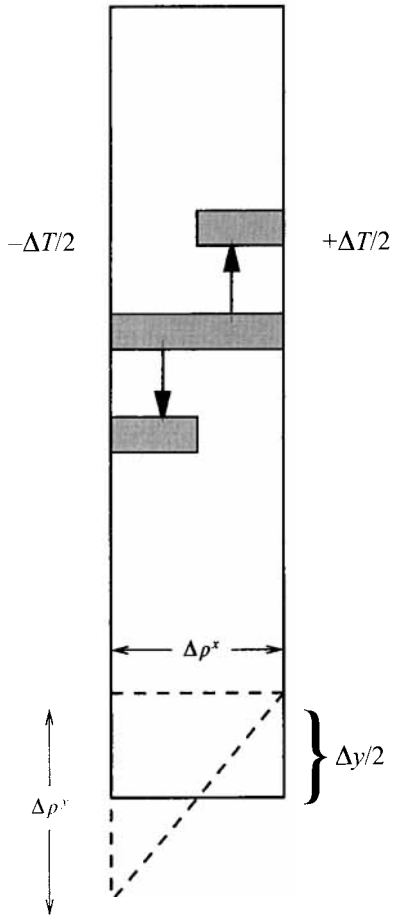

FIGURE 2. Illustration of the balancing of horizontal and vertical density differences to estimate the size of a convection roll. Grey shades represent regions of similar concentrations. The large arrows indicate how concentration is shifted by convection.

In the absence of fluid motion, $\boldsymbol{u} = 0$, (3.5) reduces to the Burgers equation. It has travelling wave solutions which describe the motion of the interface between the colloid and the supernatant (medium free from particles) (Barker & Grimson 1987; Saarloos & Huse 1990; Esipov 1995). Surprisingly, the Burgers form is not required to produce the steep concentration gradients between layers. Numerical evidence shows that steps in concentration form even when $v_0 = 0$. This suggests that the layers are formed because of the coupling between the velocity and concentration fields rather than from the simple steepening effects produced by Burgers equation.

4. The Galerkin approximation (one-dimensional reduction)

To reduce the problem to one spatial dimension we use a Galerkin-like method in the x-variable. We choose trial functions with explicit x-dependence inspired by (3.4) which we believe will approximate the real solution. Since we have restricted the form of the approximate solutions we cannot expect to satisfy the differential equations exactly, but we require that the amount by which the equations fail to hold, the residual, be constrained to be orthogonal to the trial functions (Strang & Fix 1973). In other words, multiply equations (3.3) and (3.5) in the previous section by appropriate

trial functions and integrate over the entire domain and equate the two sides. The resulting relations can be viewed as differential equations involving only one spatial variable, y.

First, we need to select a functional form for the velocity in the y-direction. To impose the no-slip condition, we require that v is zero on the boundaries; also, to form the convection cells, we would like it to be positive on the warm side and negative on the cool side (see figure 1). We choose a polynomial in x but unconstrained in y and t. Based on (3.4) we take

$$v = \tilde{u}(y,t)\,\mu_x(x), \qquad \mu(x) = \tfrac{1}{4}\left(x^2 - d^2\right)^2, \tag{4.1}$$

where the subscripts denote differentiation. To select u, we use the divergence-free condition, (4.1), and integration to get

$$u = -\tilde{u}_y(y,t)\,\mu(x). \tag{4.2}$$

The stream function ψ, is given by $\psi(x,y,t) = \tilde{u}(y,t)\mu(x)$. Note $\tilde{u}(y,t)$ is an unknown function that will appear in our final partial differential equations. In general the test functions are taken to be $\xi^y = f(y)\mu_x(x)$ for y-components and $\xi^x = -f_y(y)\mu(x)$ for x-components. Here $f(y)$ is an arbitrary function; we will take $f(y) = \delta(y)$ to simplify the integration. We substitute the velocity ansatz (4.1), (4.2) in (3.3) and integrate over the domain:

$$-\nu \int \nabla^2 \boldsymbol{u} \cdot \xi \,\mathrm{d}\boldsymbol{r} = \int \left(1 - \frac{\beta \Delta T}{2d} x\right) \boldsymbol{g} \cdot \xi \,\mathrm{d}\boldsymbol{r} - \int \frac{\Delta \rho}{\rho} c \boldsymbol{g} \cdot \xi \,\mathrm{d}\boldsymbol{r}. \tag{4.3}$$

Here $\boldsymbol{r} = (x, y)$ and pressure has been eliminated by integrating by parts (Fortin 1993).

Before we can perform the integration, we need to choose a trial function for the concentration. In the spirit of (4.2), (4.1) we decompose the concentration field into a part with no x-dependence and a small correction which is positive on one side, negative on the other and has zero derivative at the walls; this final condition reflects the fact that there are no beads moving through the walls of the test tube. Thus

$$c(x,y,t) = \tilde{c}(y,t) + \tilde{b}(y,t)\,\lambda(x), \qquad \lambda(x) = x\left(x^2 - 3d^2\right). \tag{4.4}$$

Combining this with (4.3), performing the integration and dropping the tildes, we obtain an ordinary differential equation giving u as a function of b,

$$\tfrac{1}{3} d^2 u_{yyyy} - 2u_{yy} + \frac{21}{2d^2} u = \frac{g}{2\nu}\left(\frac{9\Delta\rho}{\rho} b - \frac{7\beta\Delta T}{4d^3}\right). \tag{4.5}$$

Guided by (4.4) above, we choose two test functions for the concentration. The first, $\delta(y)$, will produce an equation for c_t; the second, $g(y) = \delta(y)\lambda(x)$, yields an equation for b_t. Following the procedure for the velocity, we get two one-dimensional partial differential equations for concentration:

$$c_t + F_y = D c_{yy}, \tag{4.6}$$

$$b_t + \frac{42D}{17d^2} b + G_y + \tfrac{3}{17} u c_y = D b_{yy}, \tag{4.7}$$

where the fluxes F and G are given by

$$F = v_0 c\left(1 - \tfrac{1}{2}kc\right) + \tfrac{4}{35} d^6 \left(3ub - \tfrac{17}{2} k v_0 b^2\right), \tag{4.8}$$

$$G = v_0 b\,(1 - kc). \tag{4.9}$$

Again we have rewritten the equations without the tildes. Equations (4.5)–(4.9) will be solved numerically.

These equations can be made dimensionless by defining a 'typical' convection velocity $U = \beta\Delta T g d^2/\nu$. Then we can rescale, $ud^3/U \to u$, $bd^5/a^2(\nu_0/U) \to b$, $c/c_0 \to c$, $t\nu_0/d \to t$ and $y/d \to y$. With this rescaling, all variables are $O(1)$ and there are only three parameters in the system.

In light of the discussion of the tilt of the interface we do not expect that the solutions of our reduced system will have discontinuities. The transition in the one-dimensional equations should be of approximately the length $2d\phi$, where ϕ is given by (3.6). This expectation was borne out in our numerical experiments, within a factor of 2 or so. Because the transitions are still quite sharp we refer to them as shocks, even though near-shocks is what they appear to be.

4.1. *Alternative one-dimensional formulations*

In addition to the Galerkin approach, there are several other methods we can apply to reduce the two-dimensional equations. Although we used the Galerkin equations exclusively for the numerics, we will present a few alternatives here in the hope that one may lend itself to a theoretical analysis of the system.

The collocation method requires that the equations are satisfied exactly at n points, where n is the number of unknowns. To apply this, we found it convenient to eliminate the pressure term in the velocity equation by taking a curl of it to get

$$\nu\nabla^2(v_x - u_y) + \frac{\beta\Delta T}{d}g + \frac{\Delta\rho}{\rho}gc_x = 0. \tag{4.10}$$

We now substitute the same forms for u, v, c given by (4.2), (4.1), (4.4) as were used in the Galerkin derivation into (4.10) and (3.5). This gives a velocity and a concentration equation with explicit x-dependence:

$$\nu\left[6u + 2u_{yy}(3x^2 - d^2) + \mu(x)u_{yyyy}\right] + \frac{\beta\Delta T}{d}g + 3\frac{\Delta\rho\mu_x(x)}{\rho x}gb = 0, \tag{4.11}$$

$$(c + b\lambda)_t - \frac{3\mu_x(x)}{4x}bu_y - D\left(6bx + c_{yy} + \lambda b_{yy}\right) + \left[(1 - 2c - 2bz)v_0 + u\mu_x(x)\right](c + \lambda b)_y = 0. \tag{4.12}$$

Since we have one velocity variable and two concentrations, we will pick one point for (4.11) and two points for (4.12). The natural choice for the velocity equation is $x = 0$ which gives the same form as (4.5) with slightly different coefficients. For the concentration equation, we have two options. We can pick two points where (4.12) is satisfied, or we can choose one point for which (4.12) and x-derivative of (4.12) are satisfied. In the first case, we could choose Gauss points, $x = \pm(0.577...)d$. The second option, satisfying the equation and the derivative at $x = 0$, produces a concentration equation for c,

$$c_t + [v_0 c(1 - kc)]_y + \tfrac{3}{4}d^6 bu_y = Dc_{yy}, \tag{4.13}$$

and one for b which is in the same form as (4.7) with different coefficients. The c-equation has been written out since it has different nonlinear terms from the Galerkin c-equation.

Another approach is the control volume method (Finlayson 1972). Here we start with (4.11) and (4.12); however, instead of evaluating the function at specific points,

we integrate over x. For the velocity equation this gives

$$\tfrac{2}{15}d^2u_{yyyy} + \frac{6}{d^2}u = \frac{g}{\nu}\left(\frac{2\Delta\rho}{\rho}b - \frac{\beta\Delta T}{d^3}\right).$$

This is similar to the Galerkin method since we have essentially multiplied by a constant test function and eliminated everything orthogonal to a constant. Since we need two concentration equations, we use (4.12) twice: first we integrate over x and second we multiply by x (or some other higher-degree polynomial) and integrate. Not surprisingly, the first integration yields exactly the same result as the Galerkin method (4.6). The second gives us slightly different coefficients for the b-equation. Note that this set only differs significantly from the Galerkin equations in the lack of a second-order term in the velocity equation.

4.2. *Linearized equations*

One can calculate approximately how fast disturbances will propagate by linearizing the system. In this rough estimate, we will consider u to be function of b, $u = u(b)$, a reasonable simplification for moderate- and long-wavelength variations in u. Thus we treat c and b as our independent variables here. Also we will take $D = 0$ for simplicity. Linearizing (4.6)–(4.9) gives the system

$$\begin{pmatrix} c \\ b \end{pmatrix}_t + \begin{pmatrix} v_0(1-kc) & \frac{4}{35}d^6(3u - 17kv_0b) \\ \frac{3}{17}u - v_0kb & v_0(1-kc) \end{pmatrix}\begin{pmatrix} c \\ b \end{pmatrix}_y = 0 \tag{4.14}$$

where the eigenvalues of the 2×2 matrix are the speeds of propagation. Assuming that $v_0 \ll u$ and $b \ll u$ we can calculate the eigenvalues:

$$\lambda \sim \pm\tfrac{1}{4}d^3u. \tag{4.15}$$

This is in order of magnitude agreement with the numerical solution of the complete nonlinear system. Note that disturbances propagate both up and down.

5. Discretized model

The Galerkin equations are solved numerically using a finite difference scheme. We use a variable $u_2 = \partial_y^2 u$ to change the fourth-order velocity equation into two second-order equations. All four variables, c, b, u and u_2, are knot centred. The fluxes, F and G, are computed at the centre of the intervals using averaged variables, e.g.

$$c_{i+1/2} = \tfrac{1}{2}(c_i + c_{i+1}).$$

Since the solutions will have shocks or near-shocks, we know that the computations are susceptible to numerical difficulties due to overshoot at the shock. Because of the change in the geometry from a tube to a slab and because of the simplifications made, we should expect only qualitative agreement with experiments.

The overshoot at the interfaces can be controlled by increasing D. To reduce D to a physical value, most computations were run with local diffusion where the diffusivity was chosen based on an up-winding scheme. Given a system

$$\boldsymbol{c}_t + \begin{pmatrix} 0 & \alpha \\ \beta & 0 \end{pmatrix}\boldsymbol{c}_y = 0$$

where $\boldsymbol{c} = \begin{pmatrix} b \\ c \end{pmatrix}$, we can change variables to $w = b - (\alpha/\beta)^{1/2}c$ and $v = b + (\beta/\alpha)^{1/2}c$.

The resulting system

$$\begin{pmatrix} w \\ v \end{pmatrix}_t + \begin{pmatrix} -(\alpha\beta)^{1/2} & 0 \\ 0 & (\alpha\beta)^{1/2} \end{pmatrix} \begin{pmatrix} w \\ v \end{pmatrix}_y = 0$$

can be discretized using standard up-winding techniques. When we convert the discretized system back to the original variables, we find that the up-winding adds an extra diffusive term of the form $(\Delta y(\alpha\beta)^{1/2}/2)\, c_{yy}$. This numerical diffusion is only needed in the vertical direction and can be restricted to the area around the shocks. Specifically, the vertical diffusivity (i.e. the coefficient of c_{yy}) was chosen to be

$$D_{\text{vert}} = D + \frac{u\Delta y}{2} \boldsymbol{\Theta} \cdot \begin{pmatrix} |\Delta b|^2 \\ |\Delta c|^2 \end{pmatrix}$$

where D is the physical diffusivity, u is the average velocity at the mesh point and Δy is the grid spacing. $|\Delta b|$ and $|\Delta c|$ are average jumps in b and c around the mesh point (so this correction term will be activated at the interfaces) and $\boldsymbol{\Theta}$ is a constant chosen such that $\boldsymbol{\Theta} \cdot \begin{pmatrix} |\Delta b|^2 \\ |\Delta c|^2 \end{pmatrix} \approx O(1)$ at the shocks. The averaging was done over the four nearest knots.

We use an implicit scheme for the time differencing where Δt is controlled by a step-doubling process based on the first-order backward difference method. The resulting equations are solved simultaneously via Newton's method using 1 or 2 iterations. We then use extrapolation to eliminate the first-order error in Δt, i.e. if $C(\Delta t, k)$ is the solution at the end of k time steps of size $\Delta t/k$ of the backward difference scheme,

$$C_{\text{extrapolated}} = 2C(\Delta t, 2) - C(\Delta t, 1).$$

All the computations reported here were done using a uniform spatial mesh and with the only up-winding given by the enhanced value of D.

6. Computational results

In the numerical experiments we observed both convection rolls and multiple shocks in concentration which is in agreement with physical experiments; figure 3 shows an example of typical numerical data. The two phenomena, shocks and convection, are inextricably connected, i.e. there is always a convection roll for each shock and vice versa. The number of shocks and their amplitude is extremely sensitive to changes in ΔT and perturbations in the initial conditions.

All numerical experiments shown here were run with $d = 0.4$ cm, $H = 25$ cm, $\nu = 0.01\ \text{cm}^2\,\text{s}^{-1}$, and $\beta = 2.2 \times 10^{-4}\ \text{K}^{-1}$, (the values for ν and β correspond to water), $D = 5 \times 10^{-8}\ \text{cm}^2\,\text{s}^{-1}$, $v_0 = 1.323 \times 10^{-6}\ \text{cm}\,\text{s}^{-1}$, and $\Delta T = 0.005$ K (unless indicated otherwise).

6.1. *Convergence studies*

Nonlinear first-order conservation laws frequently have non-unique solutions, only one of which is physically relevant. The solution of interest is usually the one that can be viewed as being the limit of solutions for which diffusion is getting smaller and smaller. There is always the concern that a numerical algorithm may converge to a solution other than the one that is physically relevant. Although we have less than a complete theoretical understanding of the reduced system we are solving, we did some tests to see how the solutions varied as D was decreased. Let N denote

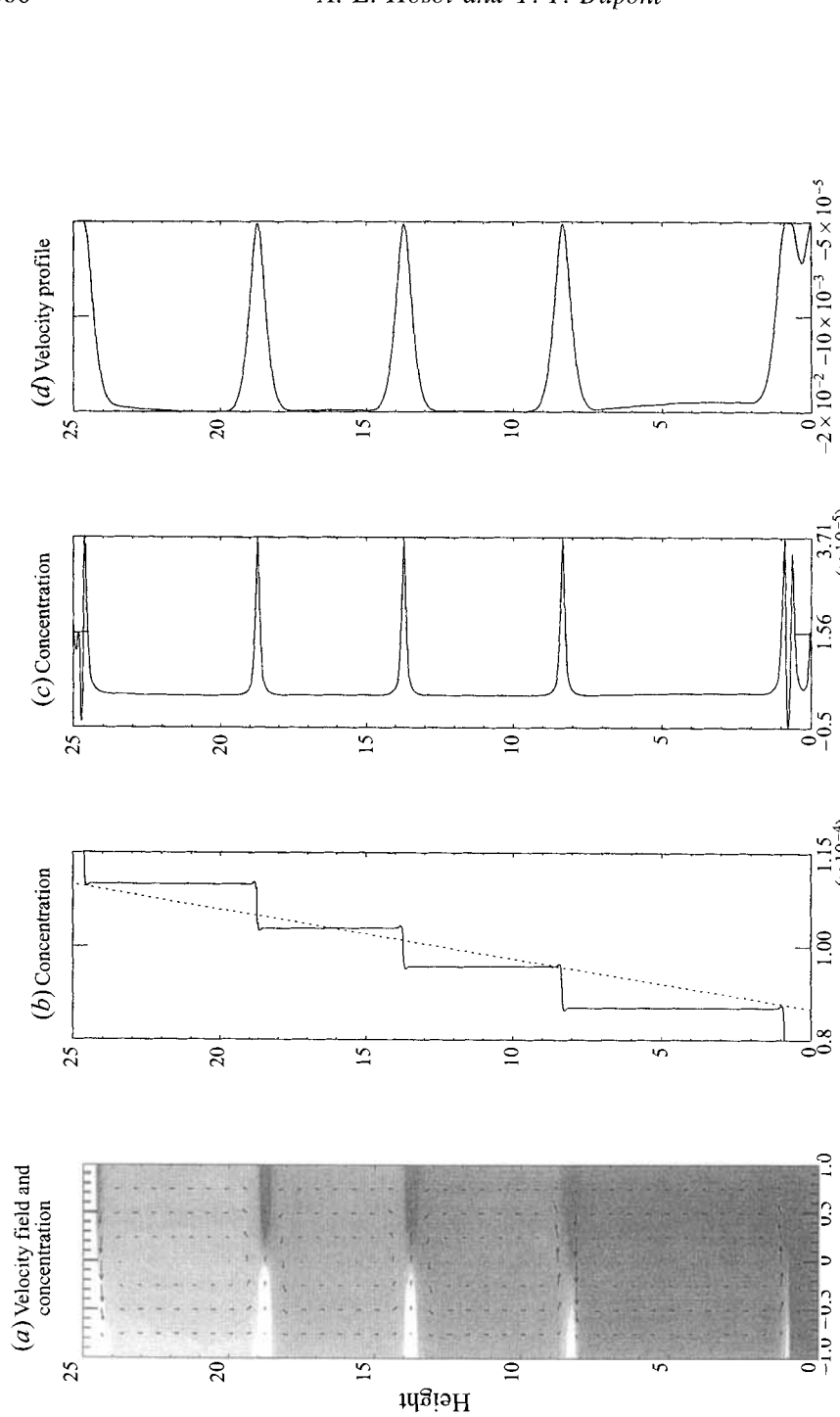

FIGURE 3. A typical example of our numerical results. (*a*) A graphic representation of what the data would look like in an actual experiment; the arrows represent the velocity field and the shading represents concentration (dark = low concentration, light = high concentration). The dotted line in (*b*) shows the initial concentration; b_{initial} and u_{initial} are zero. The number of intervals $N = 2000$; $k = 2$.

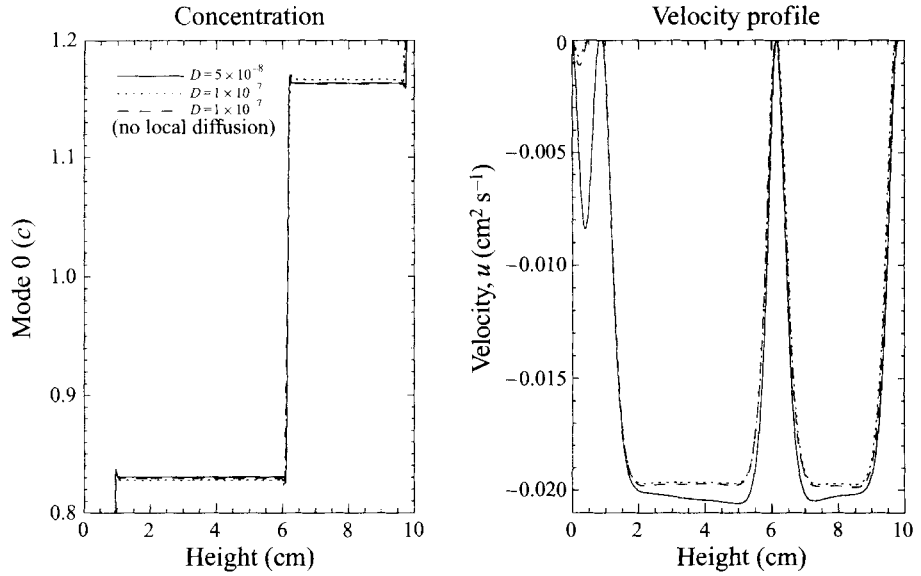

FIGURE 4. A demonstration that local diffusion stabilizes the calculation without dramatically altering the solution. Additionally, by comparing the two cases that include local diffusion, we see that the numerics are resolving the diffusion and therefore we are converging to a reasonable solution. The case with no local diffusion was run with $N = 2 \times 10^4$ and the two cases with local diffusion were run with $N = 3200$.

the number of mesh points in the computation. To test the effects of local diffusion, we ran a test case with $N = 2 \times 10^4$, $D = 10^{-7}$ cm^2 s^{-1}, and no local diffusion; the diffusion should be resolved at this fine discretization. This was compared to the case with $N = 3200$ and $D = (10^{-7} + \text{local})$ cm^2 s^{-1} using locally enhanced diffusion. Some of the results of these studies are shown in figure 4.

Another test one normally performs is gradually refining the mesh to check convergence (figure 5). This case demonstrates that the 'glitch' at the edge of the shocks appears to be real, at least for our reduced system. In all four cases the bump is smooth and wider than the mesh spacing. This indicates that the bump is probably not the result of under-resolving the near-shock. This could come from the reduction process, or it may be present in the full system; we are not sure.

6.2. *Initial conditions*

We have only seen multiple shocks in our model when there is some perturbation superimposed on uniform initial conditions. Two variations we tried were: (i) a sine wave superimposed on a flat initial concentration and (ii) a uniform gradient in concentration. In the first case, we varied the period of the sine wave to get 2–25 cycles per tube; the amplitude of the perturbation varied between $0.1c_0$ and $0.01c_0$. One interesting feature in these cases is that the number of shocks produced does not correspond directly with the period of the initial perturbation (see figure 6). This indicates that the shocks are not formed by a simple steepening of initial fluctuations as one would expect in a pure Burgers system. We also observe that the shocks usually do not merge (see below) which indicates that effective repulsion is achieved by the presence of convection rolls.

The tilted initial condition was motivated by experiments done by Siano (1979) in which linearly varying the initial concentration lead to much more rapid formation of multiple shocks. An example of this initial concentration is shown in figure 3(*b*) as a

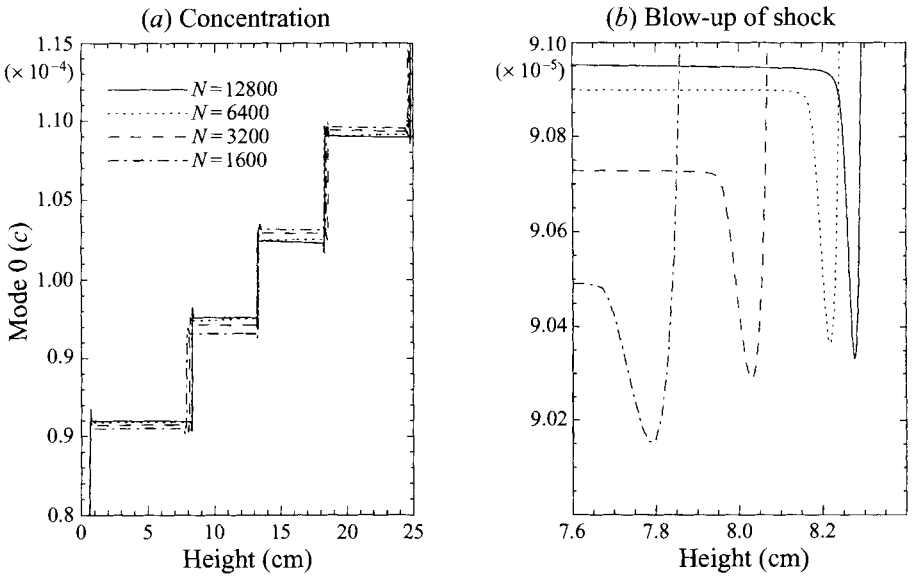

FIGURE 5. (*a*) The effects of an under-resolved spatial discretization; (*b*) demonstrates that the 'glitch' at the edge of the shocks is real in our reduced system. $k = 2$.

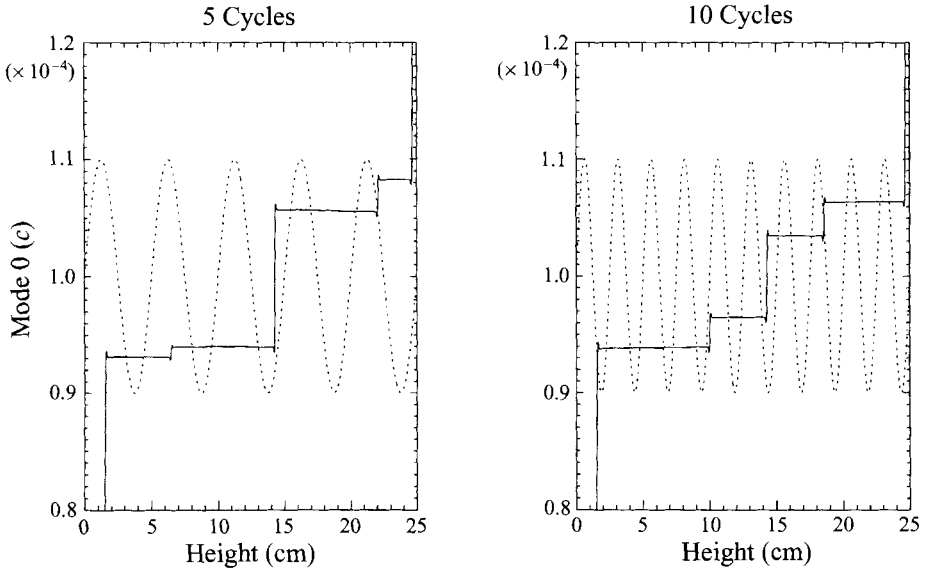

FIGURE 6. Plots showing that the number of cycles in the initial perturbation does not correspond with the number of shocks formed. This suggests that the shocks are *not* formed by a steepening of initial perturbations as one would expect in a pure Burgers system. Both final conditions are shown at $t = 10^6$ s. $N = 3200$.

dotted line. We found that there is a limited range of initial slopes in which multiple shocks are formed. This is predicted by the calculation of H_{roll} in §3: if $c_y|_{init}$ is too small, H_{roll} becomes larger than the length of the tube.

We also observed that the rolls form by 'peeling off' the ends of the tube; i.e. the initial rolls form at the top and bottom of the tube and spread until a new roll forms at the leading edges. This is illustrated by the 'waterfall' time series in figure 7

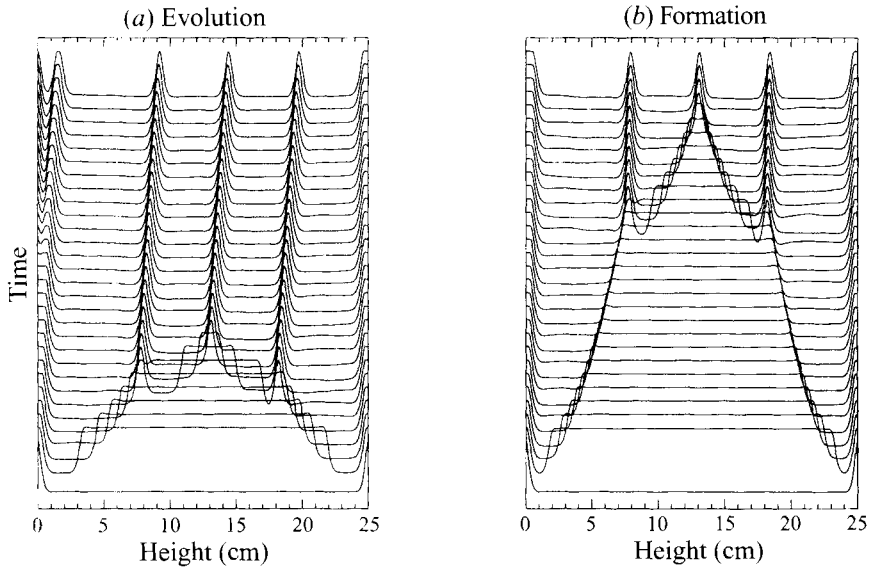

FIGURE 7. A 'waterfall' picture of a time series for velocity. The first profile is at the bottom of the plot and time increases as one moves upwards. In (*a*) the final time is 1.5×10^6 s. Plot (*b*) resolves the formation of the shocks; the first rolls form at the ends of the tube and spread until the next set peels off from the initial rolls. The final time here is 5×10^5 s. $N = 3200$.

which shows a succession of snapshots of the velocity profile; a small displacement of the graph of u is added to each successive output. The peaks in these graphs are locations where u gets very close to zero, i.e. these are the interfaces between rolls. The 'Evolution' figure shows the behaviour over 1.5×10^6 s, about 17 days, while the 'Formation' figure shows the first third of that.

6.3. *Comparison with experiments*

Qualitatively the simulations correspond very well with experimental data. Both multiple shocks and multiple convection rolls are observed numerically using experimental parameters (see figure 3). Siano (1979) shows that an initial concentration gradient will give rise to evenly spaced shocks which form relatively quickly (≈hours); these shocks move at approximately the creaming velocity and slowly spread apart. This is also observed in the numerics as shown in figure 8.

As mentioned in §2, the experiments are extremely sensitive to changes in ΔT. When one views the tubes for an extended period of time, the layers are destroyed by radiated body heat. Then when the observer leaves, the layers are reformed in approximately the same position. This is also seen numerically where the 'observer' is simulated by increasing the temperature on one side of the tube for a few minutes. In this case we see that the layers are not completely destroyed but are 'smeared out' so that the interfaces are no longer easily visible. Thus when the shocks are reforming there is already an initial perturbation that causes them to reappear in their original configuration.

Apart for the differences in geometry a quantitative comparison is much more problematic due to difficulties in both the numerics and the experiments. Experimentally, one runs into trouble because the temperature gradient is small; without special equipment it is rather difficult to measure a temperature difference ≈ 0.01 K and maintain it during the weeks that the experiment is run. Numerically a quantitative comparison may be difficult because of the assumptions made in the reduced model.

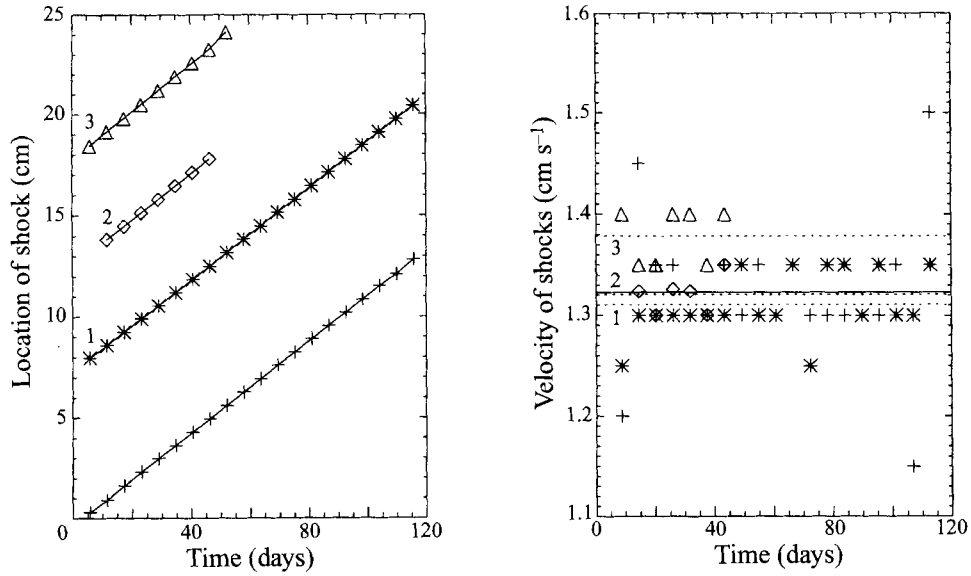

FIGURE 8. Evenly spaced shocks are produced which rise at approximately the creaming velocity. The solid line represents v_0. We also see from the average velocity of each interface (shown by the dotted lines) that they are slowly spreading apart. Different symbols represent different shocks from one simulation.

First, we have assumed a two-dimensional system and neglected the geometry of the test tube. This could be corrected by choosing appropriate basis functions for a cylindrical tube and applying the same techniques described in §4. Additionally, we would expect the time scales in the numerics to differ from experimental values since we have only included the slowest decaying mode, b, in our expansion for concentration.

7. Concluding remarks

We have presented a model of sedimenting/creaming colloids which provides a possible explanation of the formation of multiple layers or shocks. Our model produces the experimentally observed structures. These structures appear to be formed due to a balance between creaming and convection driven by temperature differences and buoyancy. We have also shown that the physics can be reasonably represented using a one-dimensional approximation which allows us to study the evolution of shocks and sheds some light on the internal structure of the layers. Some of the techniques outlined above should be applicable to other multi-dimensional systems that display primarily one-dimensional characteristics, i.e. systems that develop structure in one spatial dimension but show little variation in the others. The numerical simulations not only produce the experimentally observed layers, but also qualitatively mirror the time evolution of the shocks. Both convection cells and multiple shocks are formed which then slowly spread and rise at the velocity of sedimentation or creaming.

However, more work needs to be done before we can obtain a quantitative comparison with experimental data. The width of the layers is highly sensitive to changes in ΔT and perturbations in the initial conditions; more experimental measurements

are necessary before these comparisons can be made. Additionally, we would like to understand the equations analytically.

We are also interested in combining the present study with the effect of polydispersity (Esipov 1995) which may provide a description of the evolution of the size distribution function inside the rolls.

One can view some of the results of the simulations reported here by visiting the URL `http://www.cs.uchicago.edu/~hosoi`.

Thanks to S. Esipov for his contributions in formulating the model and assistance with the literature. It is also our pleasure to acknowledge the experimental results of J. Crocker, D. Grier and D. Mueth and the enlightening discussions with all of the above plus M. Brenner, L. Kadanoff and H. Stone. This work made use of MRSEC Shared Facilities supported by the National Science Foundation under Award Number DMR-9400379 and was partially supported by ONR-AASERT N00014-94-1-0798

REFERENCES

BARKER, G. O. & GRIMSON, M. J. 1987 *J. Phys.* A: *Math. Gen.* **20**, 305.

BATCHELOR, G. K. 1972 *J. Fluid Mech.* **52**, 245.

BREWER, W. H. 1884 *Mem. Nat. Acad. Sci. USA* **2**, 165.

BURGERS, J. M. 1974 *The Non-linear Diffusion Equation.* Reidel, Dordrecht.

ESIPOV, S. E. 1995 *Phys. Rev.* E **52**, 3711.

FINLAYSON, B. A. 1972 *The Method of Weighted Residuals and Variational Principles, with Application in Fluid Mechanics, Heat and Mass Transfer.* Academic.

FORTIN, M. 1993 *Acta Numerica.* Cambridge University Press.

LANDAU, L. D. & LIFSHITZ, E. M. 1987 *Fluid Mechanics,* 2nd edn. Pergamon.

MASON, M. & MENDENHALL, C. E. 1923 *Proc. Natl Acad. Sci.* **9**, 202.

MENDENHALL, C. E. & MASON, M. 1923 *Proc. Nat. Acad. Sci.* **9**, 199.

MUETH, D. M., CROCKER, J. C., ESIPOV, S. E. & GRIER, D. G. 1996 *Phys. Rev. Lett.* **77**, 578.

NICOLAI, H., HERZHAFT, B., OGER, L., GUAZZELLI, E. & HINCH, E. J. 1995 *Phys. Fluids* **7**, 12.

SAARLOOS, W. VAN & HUSE, D. A. 1990 *Europhys. Lett.* **11**, 107.

SIANO, D. B. 1979 *J. Colloid Interface Sci.* **68**, 111.

STRANG, G. & FIX, G 1973 *An Analysis of the Finite Element Method.* Prentice-Hall.

WHITHAM, G. B. 1974 *Linear and Nonlinear Waves.* Wiley.